Mesh parameters influence on transparent and active antennas performance at microwaves

Alexis Martin, Xavier Castel, Mohamed Himdi, Olivier Lafond

Mesh parameters influence on transparent and active antennas performance at microwaves

Alexis Martin, Xavier Castel,[a] Mohamed Himdi, and Olivier Lafond
IETR, UMR-CNRS 6164, 18 rue H. Wallon, 22004 Saint-Brieuc & 263 avenue Gal Leclerc, Université de Rennes 1, 35042 Rennes, France

(Received 22 March 2017; accepted 17 July 2017; published online 29 August 2017)

Optically transparent and active square loop coplanar antennas operating in *X*-band are investigated in this letter. The frequency tunability is provided by a surface mounted beam-lead varactor with micrometric size, thereby no-visible to the naked eye. The influence of the metal mesh parameters on the sheet resistance (from 0.05 Ω/sq to 0.54 Ω/sq), the optical transparency (from 66% to 89%) and the microwave performance (return loss, resonance frequency, radiation pattern and gain) of such antennas is evaluated, compared with those of an opaque counterpart, and finally discussed. This study paves the way of their promising implementation on new surfaces, namely building and car windows for future wireless communications systems. [http://dx.doi.org/10.1063/1.4985746]

Nowadays the development of wireless communications and wireless sensors requires emerging technologies to enhance the communication network performance, especially in dense urban areas. An attractive possibility concerns the development of optically transparent antennas to improve their location in the cities by accessing new surfaces, namely glazed surfaces such as building and car windows. These antennas can be elaborated from transparent and conducting layers printed on such glass substrates. The most usual material belongs to the transparent and conducting oxide (TCO) family, namely indium tin oxide (ITO).[1–5] Hybrid solutions based on TCO materials and ultrathin metal films are also available[6–10] such as ITO/metal/ITO multilayers[11] or AgHT films (ITO/silver multilayers printed on polyester substrates).[12,13] Nevertheless the related ohmic loss and skin depth loss at microwaves are restrictive for antenna applications. In addition, optical transparency depends on the wavelength value in the visible light spectrum due to interference fringes. Moreover ITO is based on a critical raw material, namely indium.

An alternative solution has been developed specifically in our Laboratory. It is based on micrometric mesh metal films printed on glass substrates.[14] Metal layers exhibit low sheet resistance (and low ohmic loss as a result) and apertures inside the metal layers give the needed and constant optical transparency in the visible light spectrum (no interference fringes). Metal thickness adjustment prevents any skin depth effect at the operating frequency without affecting the optical transparency level.[14] Optically transparent passive antennas have already been developed from such a material at various frequencies,[15–18] thereby demonstrating the full relevance of this new technology. Now the main challenge consists in making such transparent antennas active, i.e. being tunable in terms of operating frequency[19,20] while keeping up a high level of optical transparency and microwave performance. For this purpose, a surface mounted beam-lead varactor with micrometric size has been used and implemented on such antennas to provide frequency tunability without changing their overall transparency.[21] This tunability is relevant in X-band for radar or satellite communication applications. The present work focuses on the mesh parameters influence on the active antenna performance in terms of sheet resistance value in DC mode, optical transparency in the visible light spectrum

[a]Electronic mail: xavier.castel@univ-rennes1.fr

and microwave behavior in *X*-band (from 8 GHz to 11 GHz). To this end, three transparent antennas have been fabricated with different mesh parameters, characterized and compared to an opaque counterpart.

The active antenna design is detailed in Ref. 21. It is a square loop coplanar antenna[22] (Fig. 1) consisting of different parts, namely the feeding line, the quarter wavelength matching line and the square radiating element. The coplanar waveguide (CPW) structure is selected here to clearly help the fabrication of the transparent antennas. Indeed only one side of the glass substrate needs to be coated by the transparent and conducting layer. The substrate used here is a 50.8 mm × 50.8 mm × 0.7 mm 1737 Corning glass with the following dielectric characteristics: $\epsilon_r = 5.7$ and $\tan(\delta) = 0.006$ at 2 GHz. The conducting layer is a 2 μm-thick silver film (the best electrical conductor of the periodic table: $\sigma_{Ag} = 6.1 \times 10^7$ S/m at room temperature[23]) three times thicker than the skin depth value at 10 GHz ($\delta = 0.64$ μm), as follows:[11]

$$\delta = \sqrt{\frac{1}{\mu_0 \pi f \sigma}} \tag{1}$$

where μ_0 is the permeability of the free space, f is the operating frequency and σ is the conductivity of the layer.

Three mesh antennas (optically transparent) and a continuous reference counterpart (optically opaque) have been fabricated with the process fully described elsewhere.[14] An ultrathin titanium underlayer (5 nm-thick) and a continuous silver film (2 μm-thick) are first deposited by the RF sputtering technique at room temperature. The titanium underlayer is used here only to ensure the strong adhesion of the silver overlayer onto the glass substrate. Subsequently a standard photolithographic wet etching process with the appropriate photomasks is used to fabricate the four samples: a specific mesh one for each transparent antenna and a continuous one for the reference antenna. Afterwards, stripping of the photoresist leaves each antenna pattern with a periodic array of apertures in the metal layers for the transparent antennas (see inset in Fig. 1). Each periodic array is characterized by silver strip widths s_x and s_y, and pitches p_x and p_y in the x and y directions, respectively (Fig. 1). Finally a MA46580-1209 beam-lead varactor (outside dimensions: 210 μm × 610 μm) from the M/A-COM Company is soldered with a heat-conductive paste in the middle of the upper slot of the radiating part of the antennas (where the electromagnetic field is the strongest). Its capacity value varies from 0.87 pF to 0.17 pF under an external applied DC bias voltage ranging from 2 V to 12 V, respectively. The mesh parameters of each transparent antenna are detailed in Table I.

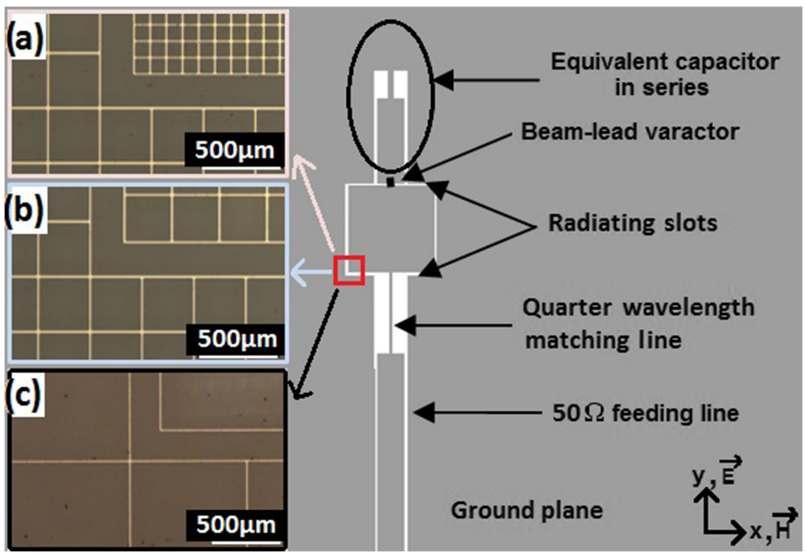

FIG. 1. Layout of the transparent frequency-tunable coplanar antenna. Detail of the mesh silver film in inset for (a) Antenna 1, (b) Antenna 2 and (c) Antenna 3.

TABLE I. Mesh parameters and related theoretical antenna characteristics.

	Antenna 1	*Antenna 2*	*Antenna 3*
Ground plane (50.8 mm × 50.8 mm)			
Pitch p_x/p_y (μm)	320/340	320/340	1015/1020
Silver strip width s_x/s_y (μm)	15/20	15/20	15
Sheet resistance R'_{sx}/R'_{sy} (Ω/sq)	0.13/0.18	0.13/0.18	0.54/0.54
Optical transparency T (%)	82.7	82.7	89.5
Feeding line (1.44 μm × 17.88 μm)			
Pitch p_x/p_y (μm)	95/100	290	715/1015
Silver strip width s_x/s_y (μm)	15	15	15
Sheet resistance R'_{sx}/R'_{sy} (Ω/sq)	0.05/0.05	0.15	0.38/0.54
Optical transparency T (%)	66.0	82.9	88.9
Quarter wavelength matching line (0.1 mm × 4.5 mm)			
Pitch p_x/p_y (μm)	90/110	90/300	90/900
Silver strip width s_x/s_y (μm)	15	15	15
Sheet resistance R'_{sx}/R'_{sy} (Ω/sq)	0.05/0.06	0.05/0.16	0.05/0.48
Optical transparency T (%)	66.3	73.0	75.5
Square radiating element (4.7 mm × 4.7 mm)			
Pitch p_x/p_y (μm)	100	290	940
Silver strip width s_x/s_y (μm)	15	15	15
Sheet resistance R'_{sx}/R'_{sy} (Ω/sq)	0.05	0.15	0.50
Optical transparency T (%)	66.6	82.9	89.2

The ground plane of the Antennas 1 and 2 is built with the same mesh parameters, and different settings are used for the other parts of the antennas. The principal aim is to ensure the strong matching of the mesh processing on each part of the antennas. According to Ref. 24, each edge of the mesh parts has to be bordered by a metal strip. Taking the feeding line as an example, the pitch of the three antennas changes from ~100 μm to ~300 μm and ~1000 μm, corresponding to $\lambda_0/300$, $\lambda_0/100$ and $\lambda_0/30$ values, respectively (λ_0 is the value of the working wavelength of the antennas at 10 GHz). Due to the lack of matching between the physical dimensions of the feeding line (1.44 mm × 17.88 mm) and the above mesh parameters, the shape of the mesh evolves from square to rectangular (see Antennas 1 and 3) to get a whole number of the elementary meshes. On the other hand, the silver strip width s can also be slightly adjusted from 15 μm to 20 μm to ensure this whole number. Finally, Antenna 3 is based on the largest mesh parameters for maximizing its optical transparency.

The sheet resistance of a square mesh metal film is computed as follows:[14]

$$R'_s = \frac{p}{s} \times R_s \tag{2}$$

where R_s is the sheet resistance of the continuous silver layer ($R_s = 8 \times 10^{-3}$ Ω/sq) before the mesh processing. In case of a rectangular mesh, the sheet resistances in x and y directions are:

$$R'_{sx} = \frac{p_x}{s_y} \times R_s \qquad R'_{sy} = \frac{p_y}{s_x} \times R_s \tag{3}$$

Therefore the sheet resistance value depends on the current propagation direction in the mesh pattern. It is worth noting that the highest sheet resistance value computed in Table I (0.54 Ω/sq) remains ~10 times lower than that of the multilayer ITO/Cu/ITO solution (4.7 Ω/sq)[11] and 15 times lower than that of the commercial solution AgHT-8 (8 Ω/sq).[12] The lowest sheet resistance value (0.05 Ω/sq) reached with the present technology will bode restricted ohmic loss for the transparent antennas.

The theoretical optical transparency T in the visible light spectrum (from 400 nm to 800 nm) of each part of antennas is computing as follows:[14]

- for a square mesh:

$$T(\%) = \left(\frac{p-s}{p}\right)^2 \times T_{sub} \times 100 \tag{4}$$

- for a rectangular mesh:

$$T(\%) = \frac{p_x - s_x}{p_x} \times \frac{p_y - s_y}{p_y} \times T_{sub} \times 100 \tag{5}$$

where T_{sub} is the optical transparency of the bare glass substrate ($T_{sub} = 0.96^2$ including the Fresnel loss of the bare glass substrate: 4% for each side). Larger the pitch is (with a constant metal strip width), higher the optical transparency level is (from 66% to 89%). Optical transparency of the bare Corning glass substrate equals 92% for comparison.

To be no-visible to the naked eye, the pitch of the mesh has to be smaller than the human visual acuity: $\theta_{min} = 4.9 \times 10^{-4}$ rad or 1.7 arcmin.[25] So depending of the location of the transparent antennas, people can be close to them (the closer distance being equal to the near point viewing distance $d = 25$ cm), and the value of the pitch to fabricate no-visible antennas will be therefore:[25]

$$p_{min} = d \times \tan(\theta_{min}) \tag{6}$$

p_{min} is thereby equal to 100 μm at the near point viewing distance and equals to 300 μm for $d = 0.6$ m.

Optical transparency of the antennas has been recorded at normal incidence by a UV-visible spectrophotometer after air (blank) calibration in the spectral range from 200 nm to 900 nm. A standard 4-point probe configuration with a regulated current source and a microvoltmeter provides the sheet resistance R_s at room temperature. The accessible area of the ground plane is sufficient for the sheet resistance measurement, contrary to the other parts of the antennas (Table I). Numerical simulations of the active antennas have been performed with a continuous silver layer (reference antenna) using the commercial CST Microwave Studio® software. The mesh antennas have not been simulated here due to the very high numerical capabilities required. Return loss, resonance frequency, radiation pattern and gain measurements of the three transparent antennas and of the opaque counterpart have been carried out in an anechoic chamber from 8 GHz to 11 GHz.

Pictures of the four antennas placed above the laboratory logo are shown in Fig. 2. The theoretical and measured optical transparencies fit well. A minor difference of about 3% is observed between the measurement and the theoretical values for Antennas 1 and 2 (Fig. 3). It is a little bit more (~6%) for Antenna 3 because the light beam size (~ 1 mm × 3 mm) of the spectrophotometer does not cross enough meshes to have a significant average of the optical transmission value. Compared to transparent and conducting solutions (such as TCO monolayers and multilayers), the transparency level remains high and constant over the entire visible light spectrum.

Sheet resistance measurement on each antenna ground plane gives: 0.0073 Ω/sq for the reference antenna; 0.19 Ω/sq for Antennas 1 and 2 and 0.91 Ω/sq for Antenna 3. These results agree well with the theoretical values (Table I), except for Antenna 3 due to an overetching effect during the fabrication process, which reduced the silver strip width from 15 μm to 10 μm. Using this last value, R'_s is therefore 0.82 Ω/sq, value closer to the measured one.

The return loss of each antenna has been measured and compared with that from numerical results (Fig. 4). It remains lower than -10 dB for all antennas and under each biasing value. The resonance frequency of the simulated antenna varies from 9.1 GHz to 10.1 GHz, corresponding to a

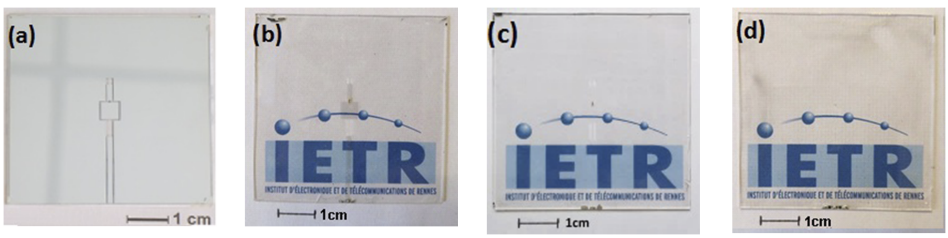

FIG. 2. Pictures of (a) reference antenna, (b) Antenna 1, (c) Antenna 2 and (d) Antenna 3.

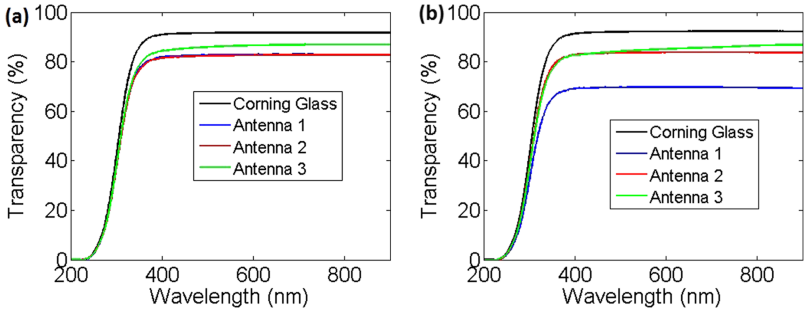

FIG. 3. Measured (a) ground plane and (b) feeding line transmission spectra of the three transparent antennas. Spectrum of the bare Corning 1737 glass substrate is also plotted for comparison.

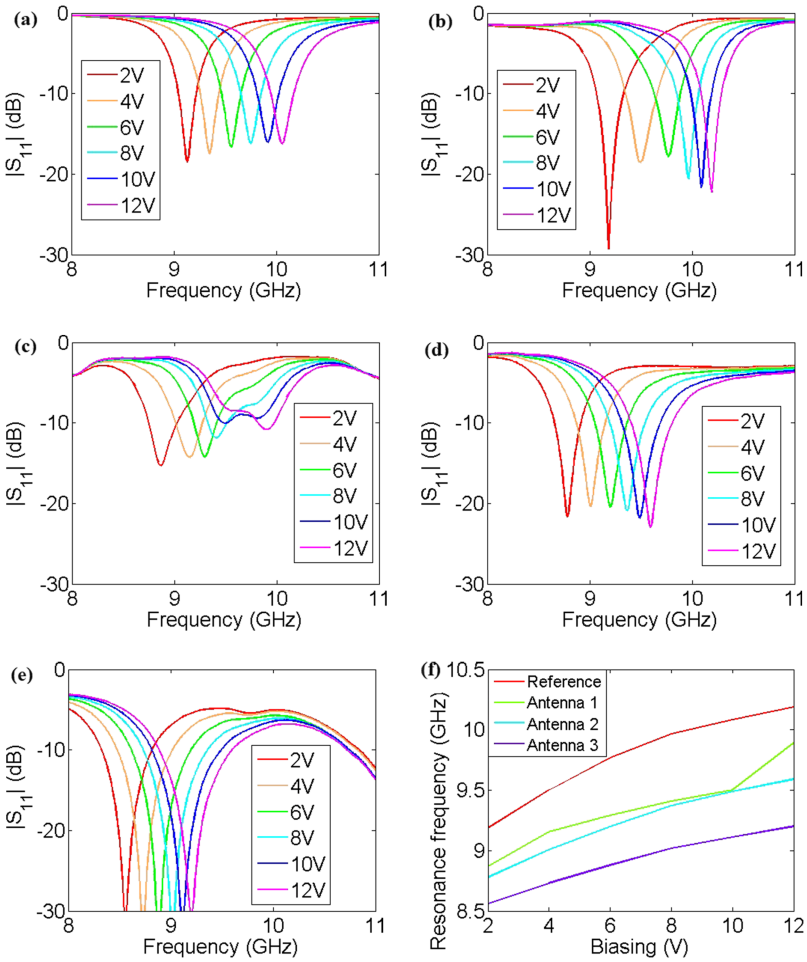

FIG. 4. Variation of the return loss versus frequency under biasing for (a) numerical results, (b) reference antenna, (c) Antenna 1, (d) Antenna 2, (e) Antenna 3. (f) Variation of the resonance frequency versus biasing for antennas under study.

theoretical frequency tunability equal to 10.4% when the varactor capacitance varies from 0.87 pF to 0.17 pF, respectively. Frequency tunability is given by the following equation:

$$Tunability\ (\%) = \frac{\Delta f}{f_c} \times 100 \tag{7}$$

where Δf is the variation of the resonance frequency, and f_c is the center frequency of the resonance frequency shift.

A very close frequency tunability behavior under biasing is measured with the reference antenna (Table II). For the transparent antennas, larger the mesh pattern is, lower the resonance frequency is under the same biasing value (Fig. 4.f) and lower the frequency tunability is. These results may be attributed to a parasitic capacitor effect due to the mesh design of the metal layer. A 400 MHz frequency shift is observed between the narrowest mesh Antenna 1 and the reference counterpart (4% of the resonance frequency); 800 MHz (8%) between the largest mesh Antenna 3 and the reference

TABLE II. Variation of the resonance frequency under biasing for antennas under study and the related maximum frequency tunability.

	Resonance frequency (GHz)	Frequency tunability (%)
Reference Antenna	9.2 - 10.2	10.3
Antenna 1	8.9 - 9.8	9.6
Antenna 2	8.8 - 9.6	8.7
Antenna 3	8.6 - 9.2	6.7

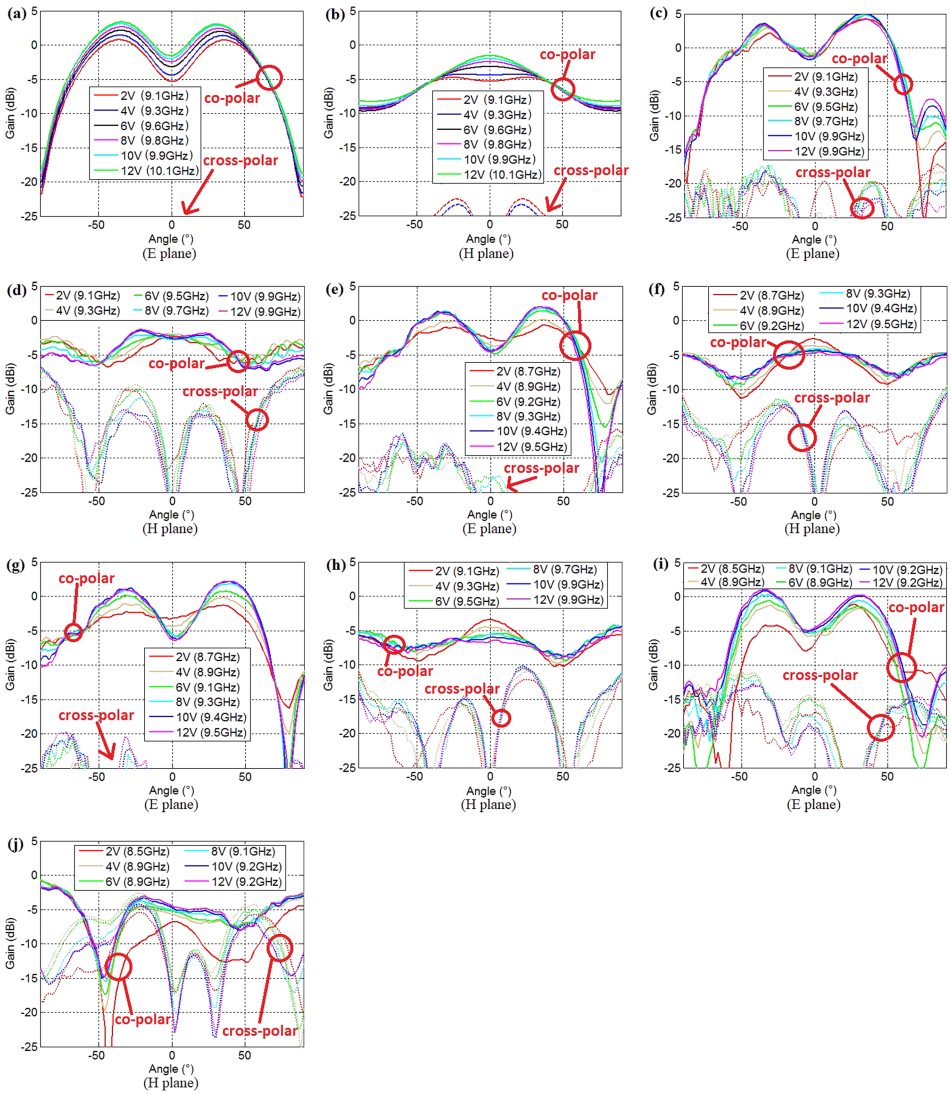

FIG. 5. E and H-plane radiation patterns versus biasing of (a-b) numerical results, (c-d) reference antenna, (e-f) Antenna 1, (g-h) Antenna 2, (i-j) Antenna 3.

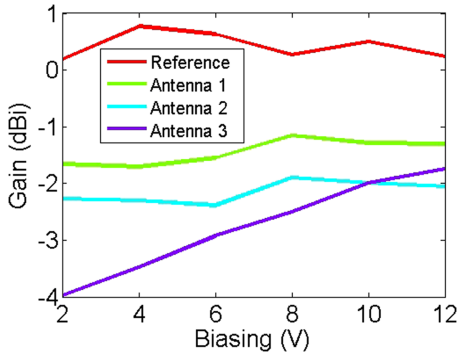

FIG. 6. Gain measurements versus biasing.

counterpart. A negligible frequency shift (lower than 100 MHz) is measured between the two transparent Antennas 1 and 2. Both of these antennas look similar with a working wavelength/pitch ratio equals to $\lambda_0/300$ and $\lambda_0/100$, respectively. Nonetheless, as mentioned in Ref. 21, a frequency shift always appears in *X*-band between the mesh antenna and the reference counterpart. And larger the pitch is, higher the shift value will be (see Antenna 3). It is worth noting that this transparent antenna is made from a mesh pattern with $\lambda_0/30$ ratio value at 10 GHz. These frequency shifts agree with the results depicted in Ref. 18, whose the narrowest mesh pattern remains closer to $\lambda_0/30$ at 24 GHz.

The radiation patterns of the antennas are shown in Fig. 5. All antennas exhibit a vertical polarization. The radiation patterns of the reference antenna and of the Antennas 1 and 2 are similar to those of the numerical results. Ripples are observed on the main E-plane lobe and are caused by the diffraction effect on the sample edges. Antenna 3 exhibits a different radiation pattern due to its slack mesh which cannot be considered as a continuous metal layer for an electromagnetic point of view. Antenna gain variation under biasing is depicted in Fig. 6. Due to the presence of ripples on the radiation patterns, the gain value is an average between the maximum value of the ripple and the gain on axis. A value close to 0.5 dBi is obtained for the reference antenna. A 2 dB lower gain is reached with Antenna 1, and 0.5 dB less with Antenna 2. Despite a negligible effect of the mesh parameter dimensions of Antennas 1 and 2 on their resonance frequency values, the use of a larger pitch induces an increase of the sheet resistance value (Table I), and thus of the ohmic loss. This behavior is fully confirmed by the microwave performance of Antenna 3. Nevertheless, transparent antennas made from such a material exhibit high microwave performance compared with those made from ultrathin metal, TCO or multilayer solutions.[11]

In this study, three transparent and active antennas have been fabricated and measured with various optical transparency and sheet resistance values. Antenna tunability is provided by a beam-lead varactor with micrometric size, thereby with a low visual impact at the near-point viewing distance, and therefore maintaining the overall antenna transparency. A frequency tunability of ~9% has been reached with satisfactory return loss and gain values in *X*-band. Accordingly, some rules are set out to design such antennas made of mesh metal films. First of all, the conducting layer needs to be thicker than three times the skin depth value at the operating frequency to suppress any skin depth loss. Then, to get a homogeneous transparent and invisible layer to the naked eye, the pitch of the mesh needs to be narrower than the visual acuity at the near-point viewing distance (25 cm) or larger if the antenna is located further away from the observer. Finally, to get a transparency and active antenna with microwave performance close to that of an opaque antenna, the pitch of the mesh needs to be smaller than $\lambda_0/100$. The width of the metal strips is determined as the best trade-off between the maximal optical transparency, the minimal sheet resistance and the ease of fabrication depending directly on the technology available in the Laboratory.

ACKNOWLEDGMENTS

This work is supported by the European Union through the European Regional Development Fund (ERDF), the Ministry of Higher Education and Research, the Région Bretagne, the Département

des Côtes d'Armor and Saint-Brieuc Armor Agglomération, through the CPER Projects 2015-2020 MATECOM and SOPHIE / STIC & Ondes.

[1] J.-A. Jeong, H.-K. Kim, H.-W. Koo, and T.-W. Kim, "Transmission electron microscopy study of degradation in transparent indium tin oxide/Ag/indium tin oxide multilayer films," Applied Physics Letters **103**, 011902 (2013).
[2] Y. Shigesato and D. C. Paine, "Study of the effect of Sn doping on the electronic transport properties of thin film indium oxide," Applied Physics Letters **62**, 1268–1270 (1993).
[3] P. F. Carcia, R. S. McLean, M. H. Reilly, Z. G. Li, L. J. Pillione, and R. F. Messier, "Low-stress indium-tin-oxide thin films rf magnetron sputtered on polyester substrates," Applied Physics Letters **81**, 1800–1802 (2002).
[4] C. Kocia and S. V. Hum, "Design of an optically transparent reflectarray for solar applications using indium tin oxide," IEEE Transactions on Antennas and Propagation **64**, 2884–2893 (2016).
[5] C. Tsakonas, S. C. Liew, C. Mias, D. C. Koutsogeorgis, R. M. Ranson, W. M. Cranton, and M. Dudhia, "Optically transparent frequency selective window for microwave applications," Electronics Letters **37**, 1464–1466 (2001).
[6] K.-H. Choi, H.-J. Nam, J.-A. Jeong, S.-W. Cho, H.-K. Kim, J.-W. Kang, D.-G. Kim, and W.-J. Cho, "Highly flexible and transparent InZnSnOx/Ag/InZnSnOx multilayer electrode for flexible organic light emitting diodes," Applied Physics Letters **92**, 223302 (2008).
[7] S. Hong, Y. Kim, and C. W. Jung, "Transparent UWB antenna with IZTO/Ag/IZTO multilayer electrode film," International Journal of Antennas and Propagation **2016**, 6751790 (2016).
[8] K. Sivaramakrishnan and T. L. Alford, "Metallic conductivity and the role of copper in ZnO/Cu/ZnO thin films for flexible electronics," Applied Physics Letters **94**, 052104 (2009).
[9] T. Minami, "Transparent and conductive multicomponent oxide films prepared by magnetron sputtering," Journal of Vacuum Science & Technology A: Vacuum, Surfaces, and Films **17**, 1765–1772 (1999).
[10] D. Sahu and J.-L. Huang, "The properties of ZnO/Cu/ZnO multilayer films before and after annealing in the different atmosphere," Thin Solid Films **516**, 208–211 (2007).
[11] F. Colombel, X. Castel, M. Himdi, G. Legeay, S. Vigneron, and E. Motta-Cruz, "Ultrathin metal layer, ITO film and ITO/Cu/ITO multilayer towards transparent antenna," IET Science, Measurement and Technology **3**, 229–234 (2009).
[12] T. Peter, T. I. Yuk, R. Nilavalan, and S. W. Cheung, "A novel technique to improve gain in transparent UWB antennas," in *2011 Loughborough Antennas Propagation Conference* (2011) pp. 1–4.
[13] M. S. A. Rani, S. K. A. Rahim, P. J. Soh, B. M. Saad, M. I. Sabran, and M. F. M. Yusoff, "A transparent UWB antenna with a 5 to 6 GHz band notch using two split ring resonators," Applied Computational Electromagnetics Society Journal **30**, 1215–1222 (2015).
[14] J. Hautcoeur, X. Castel, F. Colombel, R. Benzerga, M. Himdi, G. Legeay, and E. Motta-Cruz, "Transparency and electrical properties of meshed metal films," Thin Solid Films **519**, 3851–3858 (2011).
[15] J. Hautcoeur, F. Colombel, X. Castel, M. Himdi, and E. Motta-Cruz, "Optically transparent monopole antenna with high radiation efficiency manufactured with a silver grid layer (AgGL)," Electronics Letters **45**, 1014–1016 (2009).
[16] J. Hautcoeur, X. Castel, F. Colombel, M. Himdi, and E. Motta-Cruz, "Comparison of the microwave performance of transparent wire monopole antennas based on silver films," Journal of Electronic Materials **42**, 552–557 (2013).
[17] E. R. Escobar, N. J. Kirsch, and R. B. Turner, "Antenna array with meshed elements for beamforming applications," in *PIERS Proceedings* (2013) pp. 1356–1360.
[18] Q. H. Dao, R. Braun, and B. Geck, "Design and investigation of meshed patch antennas for applications at 24 GHz," in *2015 European Microwave Conference (EuMC)* (2015) pp. 1499–1502.
[19] B. Babakhani, S. K. Sharma, and N. R. Labadie, "A frequency agile microstrip patch phased array antenna with polarization reconfiguration," IEEE Transactions on Antennas and Propagation **64**, 4316–4327 (2016).
[20] N. C. Papanicolaou, M. A. Christou, and A. C. Polycarpou, "Frequency-agile microstrip patch antenna on a biased liquid crystal substrate," Electronics Letters **51**, 202–204 (2015).
[21] A. Martin, X. Castel, O. Lafond, and M. Himdi, "Optically transparent frequency-agile antenna for X-band applications," Electronics Letters **51**, 1231–1233 (2015).
[22] B. R. Holland, R. Ramadoss, S. Pandey, and P. Agrawal, "Tunable coplanar patch antenna using varactor," Electronics Letters **42**, 319–321 (2006).
[23] W. Haynes, *CRC Handbook of Chemistry and Physics*, 97th Edition (CRC Press, 2016–2017).
[24] J. Hautcoeur, F. Colombel, X. Castel, M. Himdi, and E. Motta-Cruz, "Radiofrequency performances of transparent ultra-wideband antennas," Progress In Electromagnetics Research C **22**, 259–271 (2011).
[25] W. N. Charman, "Static accommodation and the minimum angle of resolution," American Journal of Optometry and Physiological Optics **63**, 915–921 (1986).